layers grown during subsequent sintering cycles. Unetched specimens show that the Al_2O_3 spheres appear to intrude into the Mo grains. From the etch boundaries near to the contact areas of Al_2O_3 spheres and Mo grains it is obvious that the intrusion is a virtual effect which results from a fast deposition of material onto Mo grains at the areas away from the contact area and a negligible deposition rate at the contact area itself.

By a modified contact flattening approach based on a chemical potential increase at contact areas caused by transmitted stresses and based on diffusion of material through the thin liquid films in the contact areas of Al_2O_3 spheres and Mo, the intrusion rate of Al_2O_3 particles into Mo grains was calculated. It is found to be orders of magnitude smaller than the grain growth rate of Mo grains. The calculation and the experiments both show that the shape changes of grains due to contact flattening are negligible compared to the shape change of grains resulting from shape accommodation to the Al_2O_3 particles during Ostwald ripening.

Acknowledgements—This work was supported jointly by the Korea Science and Engineering Foundation (KOSEF) and the Deutsche Forschungsgemeinschaft (DFG). One of the authors (S.-J.L.K.) is grateful to KOSEF and DFG for financial support. Helpful discussions with Professor R. L. Coble, and Mr N. M. Hwang are acknowledged.

REFERENCES

1. See, for instance, the following references: (a) C. Wagner, *Z. Elektrochem.* **65,** 581 (1961); (b) A. J. Ardell, *Acta metall.* **20,** 61 (1972); (c) S. S. Kang and D. N. Yoon, *Metall. Trans. A* **13A,** 1405 (1982); (d) A. N. Niemi and T. H. Courtney, *J. Mater. Sci.* **16,** 226 (1981); (e) A. F. Smith, *Acta metall.* **15,** 1867 (1967).
2. S. S. Kim and D. N. Yoon, *Acta metall.* **31,** 1151 (1983).
3. S.-J. L. Kang, W. A. Kaysser, G. Petzow and D. N. Yoon, *Powder Metall.* **27,** 97 (1984).
4. S.-J. L. Kang, Y. D. Song, W. A. Kaysser and H. Hofmann, *Z. Metallk.* **75,** 86 (1984).
5. F. A. Shunk, in *Constitution of Binary Alloys,* 2nd Suppl., p. 516 McGraw-Hill, New York (1969).
6. S. S. Kim and D. N. Yoon, *Acta metall.* **33,** 281 (1985).
7. W. D. Kingery, *J. appl. Phys.* **30,** 301 (1959).
8. R. B. Heady and J. W. Cahn, *Metall. Trans.* **1,** 185 (1970).
9. F. F. Lange, *J. Am. Ceram. Soc.* **65,** C-23 (1982).
10. V. Smolej, *J. Am. Ceram. Soc.* **66,** C-33 (1983).
11. H. H. Park, S.-J. L. Kang and D. N. Yoon, *Metall. Trans.* In press.
12. S.-J. L. Kang and D. N. Yoon, *J. Mater. Sci.* in press.
13. E. D. Hondros, in *Precipitation Processes in Solids* (edited by K. C. Russell and H. I. Aaronson), p. 1. MS/AIME (1978).
14. J. E. Marion, A. G. Evans, M. D. Drory and R. D. Clarke, *Acta metall.* **31,** 1445 (1983).
15. Reply to V. Smolej by F. Lange, *J. Am. Ceram. Soc.* **66,** C-33 (1983).

APPENDIX

"Intrusion" of an Al_2O_3 particle

The chemical potential difference at and off the contact area is given by

$$\Delta\mu = \gamma_{LV}\cdot\frac{\Omega\bar{R}K_1}{2rh} - 2\gamma_{SL}\Omega\left(\frac{1}{\bar{R}}+\frac{1}{r}\right) \qquad (A1)$$

if $2r \gg h$. From $\Delta C \approx C_0\cdot\Delta\mu/RT$ we obtain the excess solute concentration in the melt

$$\Delta C \approx \frac{C_0}{R^0T}\left\{\gamma_{LV}\frac{\Omega\bar{R}K_1}{2rh} - 2\gamma_{SL}\Omega\left(\frac{1}{\bar{R}}+\frac{1}{r}\right)\right\} \qquad (A2)$$

where C_0 is the solute concentration in the melt when in contact with a plane interface of saturated solid solution, $\bar{R}$ is the average radius of the Mo grains, Ω the molar volume of Mo in the solid solution Mo(Ni), γ_{LV} and γ_{SL} are the specific interface energies of liquid/vapor and solid/liquid, r the radius of Al_2O_3 spheres, h the depth of indentation, R^0 the gas constant and T the absolute temperature. Taking the contact area H as a thin disc of liquid, the flow from the disc is given by

$$\frac{dV}{dt} \approx 4\pi\delta D\Delta C \qquad (A3)$$

where δ is the thickness of the liquid disc, D the diffusion coefficient of Mo in the melt and ΔC is given in units of m^3/m^3. The volume of the Mo grain which has to be dissolved by the intruding Al_2O_3 sphere is

$$\frac{dV}{dt} = \pi h\cdot(2r-h)\cdot\frac{dh}{dt} \approx 2\pi hr\frac{dh}{dt}. \qquad (A4)$$

Combining equation (A2), (A3) and (A4) yields equation (6).

A basic assumption for equation (6) is that the contact area is determined by the depth of indentation of the Al_2O_3 sphere into a Mo grain, as shown in Fig. 7(b). Under this condition, the material transported out of the contact area is estimated to be larger than the real volume of the indentation. However, when we think about the increase of contact area due to grain growth, such as shown in Fig. 7(a), the diffusion distance is underestimated. These two opposite effects are assumed to compensate each other in equation (6) during the early stage of grain growth.

Trapping of Al_2O_3 particle

Due to the transmission of the force F_p a nonsymmetrical position of an Al_2O_3 sphere between two Mo grains is assumed to result in an excess pressure at the larger area of

$$\Delta p_L = \frac{F_p}{\pi r^2} = \frac{K_1\bar{R}\gamma_{LV}}{r^2} \qquad (A5)$$

and an excess pressure at the smaller area of intrusion depth, h, of

$$\Delta p_S \approx \frac{F_p}{\pi h(2r-h)} \approx \frac{K_1\bar{R}\gamma_{LV}}{2rh}. \qquad (A6)$$

The difference in excess pressures results in a potential difference of

$$\Delta\mu_{SL} = \frac{K_1\Omega\bar{R}\gamma_{LV}}{2r^2h}(r-2h) \qquad (A7)$$

and a concentration difference of

$$\Delta C = \frac{K_1C_0\Omega\bar{R}\gamma_{LV}}{2r^2hR^0T}\cdot(r-2h). \qquad (A8)$$

If $2h \ll r$, equation (A8) is approximately

$$\Delta C \approx \frac{K_1C_0\Omega\bar{R}\gamma_{LV}}{2rhR^0T}. \qquad (A9)$$

The larger area is constant $2\pi r^2$. Migration of the Al_2O_3 sphere with velocity $\dot{g}$ requires a deposition rate at the larger area of

$$\frac{dV}{dt} = \pi r^2\dot{g} = 4\pi\delta D\Delta C \qquad (A10)$$

and

$$\dot{g} = \frac{2K_1\delta DC_0\Omega\bar{R}\gamma_{LV}}{r^3hR^0T}. \qquad (A11)$$

Acta metall. Vol. 33, No. 10, pp. 1927–1938, 1985
Printed in Great Britain.

0001-6160/85 $3.00 + 0.00

THE APPLICATION OF QUANTITATIVE TEXTURE ANALYSIS FOR INVESTIGATING CONTINUOUS AND DISCONTINUOUS RECRYSTALLIZATION PROCESSES OF Al–0.01Fe

J. HIRSCH and K. LÜCKE
Institut für Allgemeine Metallkunde und Metallphysik, RWTH Aachen, F.R.G.

(*Received* 24 *September* 1984)

Abstract—The textures of an Al–0.007 wt% Fe alloy after cold rolling (95% reduction) and recrystallization at different temperatures have been re-investigated by means of recently developed methods of quantitative texture analyses. 3-dimensional orientation distribution functions (ODF's) have been caculated and approximated by isotropic Gauss-model ODF's which permit a quantitative decomposition into textural components. With the help of this model the experimental ODF's are corrected with respect to systematic errors (ghost and truncation errors). By these means systematic analyses of the volume fraction, the exact position and particularly the shape and anisotropy of the scattering of the texture components are carried out. The different recrystallization textures are composed mainly of the cube orientation $\{001\}\langle100\rangle$ with different scatterings and the R orientation $\sim\{236\}\langle322\rangle$ with different positions. The analysis allows a semi-quantitative separation of the processes of continuous and discontinuous recrystallization and suggests strongly that, in discontinuous recrystallization, oriented nucleation predominates at low annealing temperatures and oriented growth at high temperatures.

Résumé—Nous avons étudié à nouveau les textures d'un alliage Al–0,007%Fe (en poids) après laminage (réduction de 95%) et recristallisation à différentes températures au moyen de méthodes d'analyse quantitative de la textures développées récemment. Nous avons calculé les fonction de répartition d'orientation tridimensionnelle (FRO) et nous les avons approximé par les FRO d'un modèle de Gauss isotrope qui permet une décomposition quantitative en composantes texturales. A l'aide de ce modèle, on peut corriger les FRO expérimentales des erreurs systématiques (erreurs de fantômes et de troncatures). On peut ainsi effectuer une analyse systématique de la fraction volumique, de la position exacte et surtout de la forme et de l'anisotropie de la dispersion des composantes de la texture. Les différentes textures de recristallisation sont composées essentiellement de l'orientation cubique $\{001\}\langle100\rangle$ avec diverses dispersions et de l'orientation $R\sim\{236\}\langle322\rangle$ avec différentes positions. Cette analyse permet une séparation semi-quantitative des phénomènes de recristallisation continue et discontinue et donne à penser fortement que, dans la recristallisation discontinue, la germination orientée prédomine aux basses températures de recuit et la croissance orientée aux températures élevées.

Zusammenfassung—Die Texturen einer 95% kaltgewalzten und bei verschiedenen Temperaturen rekristallisierten Al–0.007 gew% Fe Legierung wurden neu untersucht mit neuesten Methoden der quantitativen Texturanalyse. Dreidimensionale Orientierungsverteilungen (ODF's) wurden berechnet und durch isotrop streuende Gauss-Modell ODF's angepaßt, welche eine quantitative Zerlegung in Texturkomponenten ermöglichen. Mit Hilfe dieses Modells können systematische Fehler (Geister- und Reihenabbruchfehler) der experimentellen ODF's korrigiert werden. So konnten systematische Analysen der Mengenanteile, der exakten Position und besonders der Form und Anisotropie von Streungen der Texturkomponenten durchgeführt werden. Die verschiedenen Rekristallisationstexturen bestehen im wesentlichen aus der Würfellage $\{001\}\langle100\rangle$ mit unterschiedlichen Streuungen und der R-Lage $\sim\{236\}\langle322\rangle$ mit unterschiedlichen Positionen. Die Analyse erlaubt eine halbquantitative Trennung der Prozesse von kontinuierlicher und diskontinuierlicher Rekristallisation. Sie zeigt deutlich, daß für die diskontinuierliche Rekristallisation orientierte Keimbildung bei niedriger Glühtemperatur überwiegt und orientiertes Wachstum bei hoher Glühtemperatur.

1. INTRODUCTION

Two processes leading to a re-forming of the microstructure may take place during annealing after cold deformation. These are continuous recrystallization (also called recrystallization *in situ*) which consists of the formation and growth of subgrains and discontinuous (or genuine) recrystallization which occurs by the movement of large angle grain boundaries. Although these two modes have been known for decades [1–4], it has not been possible to distinguish unambiguously between them after recrystallization is completed. Similarities between deformation and recrystallization orientations have been used as an indication of continuous recrystallization [1, 3, 4], but in some cases discontinuous recrystallization also leads to the same orientations [1]. The main evidence for *in situ* recrystallization has been provided by

The main recrystallization texture components are the cube and R orientations. Their peak densities (Fig. 2) and volume fractions (Fig. 4) as well as the position of the skeleton lines [Fig. 3(a)] vary systematically with annealing temperature. As already demonstrated by pole figure data in [6], the intensity and volume fraction of the cube orientation are a minimum and those of the R orientation a maximum at 360°C. It will be seen also that for this temperature the recrystallization texture is quite similar to the rolling texture. Similarly the minor components and the background (BG-) component show maxima at 360°C, although the latter is somewhat smaller than that for the as-rolled state.

For 400°C, the recrystallization texture is similar to that at 360°C except for a somewhat larger cube and smaller R component. For 520°C, in contrast, the annealing texture is composed of only two components, the R component and the Cube component with some characteristic scattering. For 280°C some characteristic differences in the recrystallization texture are found. The Cube component shows extremely strong scattering in the ϕ-direction, i.e. with respect to rotations around the rolling direction (Cube_{RD} and Goss), and a component similar to the Bs recrystallization component BsR is observed. It should be emphasized that none of these additional recrystallization orientations are found after annealing at 360°C (Table 1).

4. DISCUSSION OF THE ODF ANALYSIS

4.1. Decomposition of the ODF's into isotropic Gauss components

Although ODF's provide a much clearer insight into the orientation distribution than pole figures, two major difficulties are still encountered: (i) they are rather complex 3-dimensional functions which are difficult to vizualize in Euler angle space with its distorted metrics; (ii) they contain some grave errors (truncation and ghost error) which are mainly due to the series expansion method used to reproduce the ODF's from the pole figures. For these reasons an approximation of the ODF's by model ODF's consisting of a superposition of isotropic Gauss-type

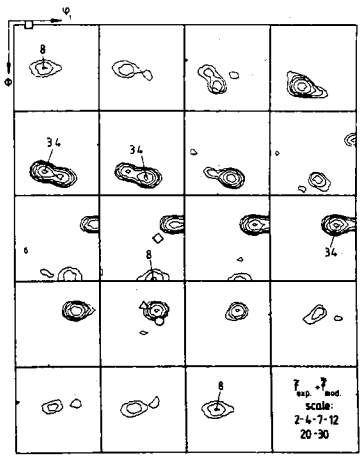

(a)

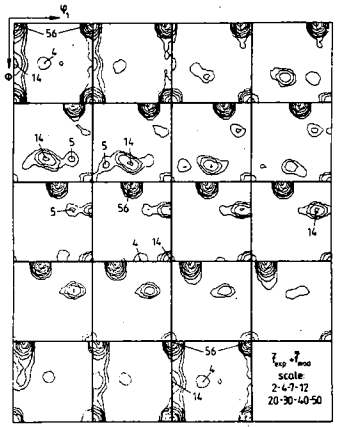

(b)

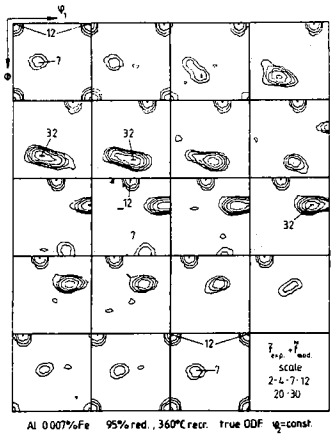

(c)

components has been applied here. This procedure which is justified by the excellent agreement between experimental and model ODF's (cf. Section 4.2) strongly reduced both difficulties and will now be demonstrated in detail. Some limitations of the model will be discussed in Section 4.3.

(a) In the form of volume fractions, M_i, of the components as given in Table 1 and Fig. 4 the method not only yields a simple, condensed and quantitative description of the texture but directly exhibits its principal features. It is superior to considerations involving only the peak height f_i since it takes into account both the width ψ_i of the peaks (which strongly influences the volume fraction by the third power, and also their anisotropic scattering. This can be done by considering the deviation of the true position g_i of the component from the symmetric position and/or by introducing auxiliary components (which may not result in a true maximum). Because of the minimization procedure the volume fractions

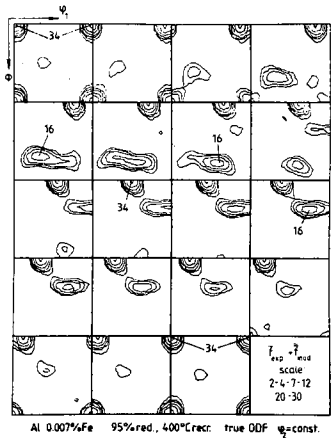

(d)

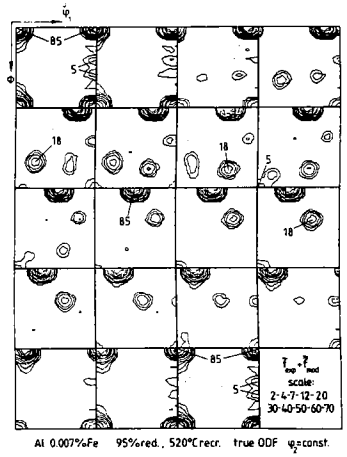

(e)

Fig. 2. (a–e) Approximate true (ghost corrected) ODF's for material rolled 95% (a) (symbols indicate 40° ⟨111⟩ rotated S components), and annealed 312 h at 280°C (b), 10 h at 360°C (c), 80 min at 400°C (d), and 60 s at 520°C (e) ($I_{max} = 22$).

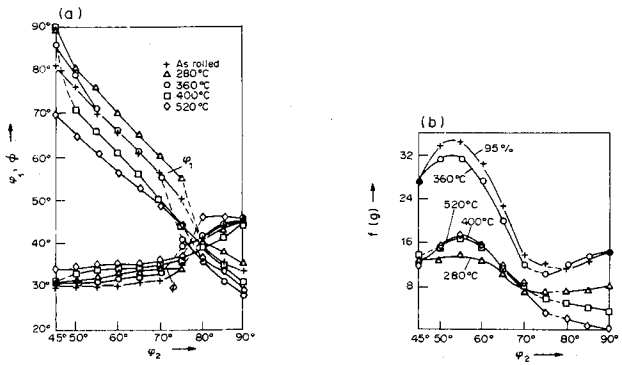

Fig. 3. (a) Path of, and (b) orientation density along, the skeleton lines ($I_{max} = 22$). The paths given by the coordinates φ_1 and ϕ of the intensity maxima in the sections $\varphi_2 = \text{const}$; the dashed sections indicate ranges in which the path of the skeleton line changes strongly.

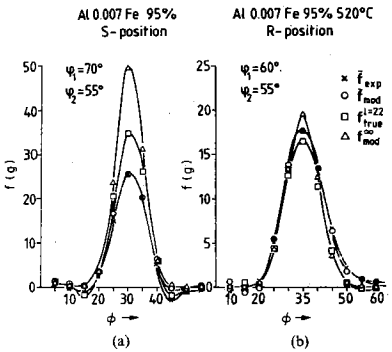

Fig. 8. (a, b) Examples of corrections to experimental ODF ($l_{max} = 22$). Reduced experimental ODF $\tilde{f}$: crosses; reduced Gauss model $\tilde{f}_{mod}$: circles; ODF after ghost correction f: squares; ODF after additional correction of the truncation error f^{∞}_{mod}: triangles (i.e. $l_{max} = \infty$). (a) S position and (b) R position for the cases shown in Fig. 7 (a, b).

with the true ODF [Fig. 2(a)] shows that most of the difference intensities lie in the near neighbourhood of the high peaks. This indicates a deviation from the ideal Gauss shape which is however small and largely due to the steep flanks of the peaks so that a small shift of the peak position leads to large differences.

In most cases the different components of an ODF lie so close together that they overlap strongly. As a result direct checking of the basic assumption that scattering about the individual components occurs according to an isotropic Gauss function is generally not possible. In the present work, however, the R component is so well separated from the others that such a check was possible. In Fig. 7(b) the experimental (crosses) and model (circles) densities around the R position are plotted for the three directions corresponding to the Euler angles and impressive agreement is obtained. In addition the Gauss distribution matches almost perfectly the measured densities for the main S component of the rolling texture [Fig. 7(a)].

Agreement of this nature justifies the use of Gauss functions or, more generally, the decomposition of ODF's into isotropic components, in more complex cases. For example, the large density differences along the skeleton line of Fig. 3(b) between 10 and 36 show immediately that superposition of components provides a better description of the rolling texture than the more or less homogeneous orientation tube proposed in [15]. Furthermore consideration of the course of the skeleton line [Fig. 3(a)], and particularly the sudden changes of φ_1 and ϕ with φ_2 at $\varphi_2 \approx 75°$ (dashed lines) together with the rather low intensity in this range [Fig. 3(b)], indicates the presence of two orientation accumulations, one around the S orientation ($\varphi_2 = 55°$), the other around the Bs orientation ($\varphi_2 = 90°$). Similar observations have been made also in rolled copper [16, 17].

4.3 Anisotropic scattering

Because the scattering of the components is not usually fully isotropic measures must be introduced into the component analysis. However the calculation effort involved is such that only isotropic model functions can be applied.

(a) For the case of small anisotropy only the isotropic model component is used which, due to the minimization procedure, averages over the different directions. Errors appear in the difference ODF's, e.g. in Fig. 6(a) and 7(a) near the S position (φ_1, ϕ, $\varphi_2 = 68.5°$, 30.6°, 56°) in the φ_1 direction positive intensities appear (i.e. the model component is too small) and in the ϕ direction negative (shaded) intensities (i.e. the model component is too large). This indicates some preferred scattering the φ_1 direction which is also found often for the R component, [except for high recrystallization temperatures, cf. Fig. 7(b)] and corresponds to a rotation around the sheet normal.

(b) If the anisotropy is too large, two overlapping isotropic components or auxiliary components can be introduced which might individually have no physical meaning. In such cases it is often useful to consider only the sum of their volume fractions in order to emphasize that physically they form only one component. An example will be given in (d) where two partial components are used to treat the Cube component.

(c) For a symmetric component anisotropic scattering can often be handled by placing the centre of the isotropic component not exactly at, but slightly removed from the experimentally observed symmetrically situated maximum. Due to the overlapping of the symmetrically equivalent components, this might still lead to an intensity maximum in the symmetrical position, but with anisotropic scattering. The amount and direction of this displacement (which can be determined once again by minimization) then provides a quantitative measure of the anisotropy. As an example the Cu position in Table 1 has been placed not at the symmetric position $\varphi_1 = 90°$, but at 88° which represents a slight rotation around the sheet normal. Since such effects are both frequent and reproducible, it must be assumed that such a shift has a physical meaning. Another example is apparent in Fig. 9 where the model component for the Cube position after recrystallization at 280°C occurs at $\phi = 85.8°$ and $\varphi_2 = 2°$ which describes a combined shift of 4.2° around the rolling direction and of 2° around the transverse direction.

(d) The Cube position often shows systematic scattering which is sometimes rather large. After recrystallization at 520°C [Fig. 2(e)], for example, scattering is observed in the φ_1 and ϕ directions corresponding to rotations around the normal and

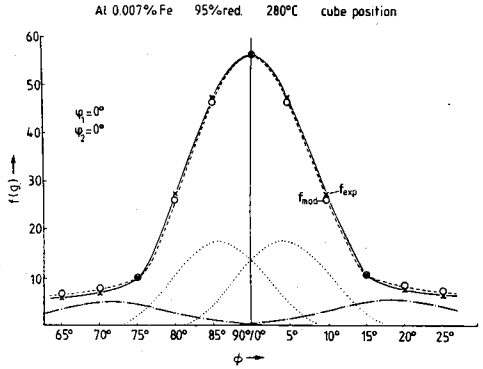

Fig. 9. True orientation density distribution $f(g)$ near the Cube position as a function of ϕ for the sample recrystallized at 280°C ($l_{max} = 22$). The observed anisotropic scattering (crosses) is described by 4 symmetrically equivalent components shifted 4.2° and 18.5° from the Cube position (circles). Two of each of these components are inserted (dotted and dashed-dotted lines).

the rolling direction. The measures described in (b) and (c) must then be applied simultaneously in order to obtain the intensity distribution. In the present texture the Cube model consists of two components ($Cube_{ND}$ and $Cube_{RD}$, Table 1). Figure 10(b) which shows the true model functions $f_{mod}(g)$ in the plane $\varphi_2 = 0°$ demonstrates the structure of the peak. The full curves give density lines for the individual components and the dashed lines the superimposed densities. It will be apparent that the complicated structural features of the peak, namely extension in the φ_1 direction close to the Cube position with a high intensity level and in the ϕ direction further away from it with a low level, are very well reproduced by the two types of Gauss components. It will be seen also from Figs 10(a) and 6(b), that the quantitative agreement with experiment is excellent.

5. DISCUSSION OF THE RECRYSTALLIZATION BEHAVIOUR

5.1. Recrystallization of the dilute Al–Fe alloys

In the recrystallization textures of rolled pure f.c.c metals with high stacking fault energy the Cube orientation is the dominant texture component and in the particular case of high purity aluminium only this component appears. Small additions of foreign atoms often lead, however, to a second texture component, the R orientation, as in the case of an alloy with only 0.004 wt% Fe in solid solution [6]. Since the R component is hardly observed in other materials, it can be assumed that its formation is related to the strong S orientation typical of the rolling texture of Al. According to Beck [1] the R component can be formed from the S component in two ways: (i) by continuous recrystallization, since both orientations, R and S, are rather similar, and (ii) by discontinuous recrystallization, since 40° ⟨111⟩ orientation relationships exist between symmetrically equivalent variants of S and R which lead to high growth rates [1, 18, 19, 20].

Ito and Lücke [5, 6] investigated the recrystallization textures of dilute Fe–Al alloys after systematic variation of the preannealing conditions, Fe content and recrystallization temperature and were able to analyze the rather complex recrystallization behaviour on the basis of the precipitation state of the iron which has a very low solubility in Al. They observed, amongst other things, the Cube component minimum near 360°C (Fig. 4) and concluded that because of the boundaries were strongly pinned by precipitation during recrystallization, continuous recrystallization was the dominant process at this temperature. At lower and higher annealing temperatures discontinuous recrystallization predominated. These unexpected findings will now be checked by a detailed analysis of the present ODF's. The physical reasons for such behaviour have been discussed in [6] and will not be treated here.

5.2. Evidence for continuous recrystallization

At 360°C the recrystallization texture is almost identical to the rolling texture. This is shown in Fig. 1(a, c) for the pole figures, Fig. 2(a, c) for the orientation densities, Fig. 3(a, b) for the position and density of the skeleton line, Fig. 4 for the volume fraction of major and minor components and in Table 1 for the orientations g_i of the main components. The background (BG) has decreased from 25% after rolling to 14% after recrystallization at

precise texture analysis of this type yields information not previously available, e.g. the volume fractions of the individual texture components, the observation of small changes in their precise positions (even if the corresponding maxima are hidden) and the anisotropy of their scattering.

These new data provide additional aids in clarifying the underlying mechanisms of recrystallization. Thus in the present work it has been possible for the first time to clearly distinguish between the separate processes of continuous (*in situ*) and discontinuous (genuine) recrystallization even after recrystallization was completed and to assess the quantitative contribution of each process.

In addition more precise details about the effects of oriented nucleation and oriented growth on the formation of the Cube and R orientations during discontinuous recrystallization have been obtained. Knowledge of the exact position of the R component and the direction of scattering of the Cube component has shown that at low recrystallization temperatures (280°C) the texture is determined mainly by nucleation processes whereas at high temperatures (520°C) selective growth of the new Cube and R grains is mainly responsible for their dominance. This is probably due to the suppression of oriented growth by the precipitation of the Fe at low temperatures before recrystallization starts [6], whereas at high temperatures (520°C) the Fe is completely in solution. Determination of the respective volume fractions at medium temperatures (360°C) has shown that recrystallization *in situ* is the dominant process. This can be attributed to precipitation during recrystallization which is known to impede grain boundary motion very effectively (Ito and Lücke [5]). The above results obtained by quantitative texture analysis have greatly increased understanding of the recrystallization processes in these alloys.

Acknowledgements—The authors wish to express their gratitude to Dr K. Ito, University of Tokyo, for valuable discussions and for supplying some of his specimens. They gratefully acknowledge the financial support by the Deutsche Forschungsgemeinschaft, Bonn-Bad Godesberg. They are indebted to the Rechenzentrum of the RWTH Aachen for making available the computer equipment and for personal assistance.

REFERENCES

1. P. A. Beck, *Phil. Mag. Q., Suppl.* **3**, 245 (1954).
2. E. Hornbogen and H. Kreye, *Texturen in Forschung und Paxis* (edited by J. Grewen and G. Wassermann), p. 274. Springer, Berlin (1968).
3. A. Ahlborn, E. Hornbogen and U. Köster, *J. Mater. Sci.* **4**, 944 (1969).
4. J. Grewen and M. V. Heimendahl, *Z. Metallk.* **59**, 205 (1968).
5. K. Ito, K. Lücke and R. Rixen, *Z. Metallk.* **67**, 338 (1976).
6. K. Ito, R. Musick and K. Lücke, *Acta metall.* **31**, 2137 (1983).
7. H. J. Bunge, *Mathematische Methoden der Texturanalyse*. Akademie, Berlin (1970).
8. R. J. Roe, *J. appl. Phys.* **36**, 2024 (1965).
9. W. Truszkowski, J. Pospiech, J. Jura and B. Major, *3ème Coll. Euro. sur les Textures...* Ponst à Mousson (1973).
10. K. H. Virnich, J. Pospiech, A. Flemmer and K. Lücke, *Proc. 5th Int. Conf. on Textures*, Aachen, Vol. 1, p. 129 (1978).
11. K. Lücke, J. Pospiech, K. H. Virnich and J. Jura, *Acta metall.* **29**, 167 (1981).
12. K. Lücke and J. Pospiech. In press.
13. J. Hirsch, M. Loeck, L. Loof and K. Lücke, *Proc. 7th Int. Conf. on Textures*, Delft (1984) In press.
14. J. Hansen, J. Pospiech and K. Lücke, *Tables for Texture Analysis of Cube Crystals*. Springer, Berlin (1978).
15. H. J. Bunge, *Z. Metallk.* **68**, 571 (1977).
16. J. Pospiech and K. Lücke, *Acta metall.* **23**, 997 (1975).
17. K. H. Virnich and K. Lücke, *Proc. 5th Int. Conf. on Textures*, Aachen, Vol. 1, p. 397 (1978).
18. B. Liebmann, K. Lücke and G. Masing, *Z. Metallk.* **47**, 57 (1956).
19. K. Lücke, *Can. Metall. Q.* **13**, 261 (1974).
20. R. Rixen, R. Musick, H. Göker and K. Lücke, *Z. Metallk.* **66**, 16 (1975).
21. I. L. Dillamore and H. Katoh, *Metal Sci.* **8**, 73 (1974).
22. A. A. Ridha and W. B. Hutchinson, *Acta metall.* **30**, 1929 (1982).
23. K. H. Virnich, G. D. Köhlhoff, K. Lücke and J. Pospiech, *Proc. 5th Int. Conf. on Textures*, Aachen, Vol. 2, p. 475 (1978).

Acta metall. Vol. 33, No. 10, pp. 1939–1943, 1985
Printed in Great Britain.

0001-6160/85 $3.00 + 0.00

MEASUREMENTS OF INTERDIFFUSIVITIES IN Cu/NiFe TERNARY ALLOY THIN FILMS

J. CHAUDHURI† and T. TSAKALAKOS

Department of Mechanics and Materials Science, College of Engineering, Rutgers, The State University of New Jersey, Piscataway, NJ 08854, U.S.A.

(*Received* 21 *August* 1984)

Abstract—Interdiffusivities have been measured in Cu/NiFe ternary alloys containing 53 at.% Cu, 40 at.% Ni and 7 at.% Fe. Isothermal anneals were performed at temperatures: 320, 345 and 400°C using thin films containing composition modulations (1.6–4.98 nm) produced by the vapor-phase growth technique. Spinodal decomposition in these films was observed in the X-ray diffraction pattern as indicated by the growth of satellite intensities at 320°C. The diffusivities at each temperature were determined from the growth or decay rate of the composition modulation. A plot of the interdiffusion coefficient $\tilde{D}_B$ versus the dispersion relation B^2 demonstrated anomalous behavior at certain wavelengths at which an enhanced elastic modulus effect is observed. The critical spinodal temperature was estimated and first three gradient energy coefficients were calculated using a nonlinear regression fit to the D_B vs B^2 curve.

Résumé—Nous avons mesuré les interdiffusivités dans des alliages ternaires Cu/NiFe contenant 53 at.% Cu, 40 at.% Ni et 7 at.% Fe. Nous avons effectué des recuits isothermes aux températures suivantes: 320, 345 et 400°C, en utilisant des films minces contenant des modulations de composition (de 1,6 à 4,98 nm) produits par la technique de croissance en phase vapeur. Nous avons observé la décomposition spinodale dans ces films par li diagramme de diffraction de rayons X qui mettait en évidence une croissance de l'intensité des satellites à 320°C. Nous avons mesuré les diffusivités à chaque température à partir de la vitesse de croissance ou de décroissance de la modulation de composition. Le tracé du coefficient d'interdiffusion $\tilde{D}_B$ en fonction de la relation de dispersion B^2 a permis de montrer un comportement anormal pour certaines longueurs d'onde pour lesquelles on observait un accroissement du module élastique. Nous avons évalué la température spinodale critique et nous avons calculé les trois premiers coefficients de l'énergie libre à l'aide d'un ajustement par régression non linéaire de la courbe de $\tilde{D}_B$ en fonction de B^2.

Zusammenfassung—Die Interdiffusion wurde in den ternären Legierungen Cu/NiFe mit 53 At.% Cu, 40 At.% Ni und 7 At.% Fe gemessen. Bei den Temperaturen 320, 345 und 400°C wurden dünne, aus der Gasphase gezüchtete Filme, die Modulationen in der Zusammensetzung aufwiesen (1,6 bis 4,98 nm), isotherm ausgeheilt. Die spinodale Entmischung dieser Filme wurde am Wachstum der Satellitenintensitäten in der Röntgenbeugung bei 320°C verfolgt. Die Diffusionskoeffizienten wurden für jede Temperatur aus Wachstums- oder Zerfallsrate der Modulation in der Zusammensetzung bestimmt. Im Diagramm des Interdiffusionskoeffizienten $\tilde{D}_B$ über der Dispersionsbeziehung B^2 fand sich bei gewissen Wellenlängen, bei denen ein verstärkter Effekt im elastischen Modul beobachtet wurde, ein anomales Verhalten. Die kritische Spinodaltemperatur wurde ermittelt. Die ersten drei aufsteigenden Energiekoeffizienten wurden mit einer nichtlinearen Regressionsanpassung und die $\tilde{D}_B/B^2$-Kurve berechnet.

INTRODUCTION

Several years ago, a technique [1, 2] was developed for producing binary alloy thin films containing short-wavelength (0.8–10 nm) composition modulations. It is well known that such a layered structure exhibits characteristic X-ray patterns with satellite reflections around the Bragg peak. The course of diffusion in modulated samples can be followed from studying the progressive intensity change of the satellite as a function of annealing time. Hilliard and his co-workers [3, 4] utilized such a technique successfully to check the modified continuum diffusion equation, which contains additional terms introduced by Hillert [5] and Cahn [6] and is the basis of the theory of spinodal decomposition. More recently, Cook *et al.* [7] derived a discrete model for the diffusion equation. In a more fundamental approach utilizing the kinetics of the Ising model, Yamauchi [8] and Khachaturyan [9] presented various theoretical models of order–disorder kinetics in a unified manner.

Tsakalakos [10, 13] observed a minimum in the diffusivity of Cu–Ni composition modulated foils at a wavelength of about 1.5 nm which could not be explained by either Cahn's continuum model or Hilliard's discrete model. Hence Tsakalakos developed a nonlinear theory of diffusion which explains successfully the stability and kinetics of the concentration waves.

Recently, there are increasing interests in studying similar diffusional effects in ternary alloys. It is thus

†Present address: Department of Mechanical Engineering, Wichita State University, Wichita, KS 67208, U.S.A.